washington.edu/datasets/eqpacislandrainindex/); this procedure allows us to align major peaks and troughs that occur within the same calendar year with adjustments that are generally less than 3 months. Because corals grow at variable rates throughout the year[29], these small chronological adjustments are reasonable and customary (and do not affect estimates of multiyear variability). Near the base of the core, an age adjustment of 1 year was needed, suggesting an age uncertainty on the full record of ±1 year. The Maiana coral grew at a rate of 7–12 mm per year; we interpolated records to a common time step of bimonthly resolution for further analysis.

Replication

The record from core MAI95-2-3 is well replicated by additional records of 65–70 years from Maiana and Aranuka, about 75 km southeast of Maiana (J.E.C. *et al.*, manuscript in preparation) and by a published 97-year record from Tarawa Atoll, about 30 km north of Maiana[4]. Correlation coefficients among coral and instrumental data over the common period 1950–89 are consistently high (Table 1), adding confidence to single-core reconstruction of regional variability in western Kiribati. We focus on the MAI95-2-3 record for further analysis because it extends the record of ENSO into pre-instrumental periods and avoids statistical nonstationarity that may be introduced through inclusion of records that differ in length. The 4-coral average correlates slightly better with instrumental data than most individual coral records, but only the MAI95-2-3 core extends the instrumental record of ENSO. Linear correlation coefficients demonstrate a strong agreement between the Maiana record and ENSO variability (Table 1), and decadal averages of the Maiana record correlate significantly over the past century (>95% confidence) with those from the Tarawa coral record and regional rainfall indices, substantiating the reality of these more subtle low-frequency signals (J.E.C. *et al.*, manuscript in preparation).

Received 1 February; accepted 9 August 2000.

1. Zhang, Y., Wallace, J. M. & Battisti, D. S. ENSO-like interdecadal variability: 1900–93. *J. Clim.* **10,** 1004–1020 (1997).
2. Trenberth, K. E. & Hurrell, J. W. Decadal atmosphere-ocean variations in the Pacific. *Clim. Dyn.* **9,** 303–319 (1994).
3. Ebbesmeyer, C. C. *et al.* in *Proc. 7th Annu. Pacific Climate (PACLIM) Workshop* (eds Betancourt. J. L. & Sharp, V. L.) 120–141 (Interagency Ecological Studies Program Technical Report No. 26, California Dept of Water Resources, Sacramento, 1991).
4. Cole, J. E., Fairbanks, R. G. & Shen, G. T. The spectrum of recent variability in the Southern Oscillation: results from a Tarawa Atoll coral. *Science* **262,** 1790–1793 (1993).
5. Graham, N. E. Simulation of recent global temperature trends. *Science* **267,** 686–671 (1995).
6. Trenberth, K. E. & Hoar, T. W. The 1990–1995 El Niño-Southern Oscillation event: Longest on record. *Geophys. Res. Lett.* **23,** 57–60 (1996).
7. Rajagopalan, B., Lall, U. & Cane, M. A. Anomalous ENSO occurrences: an alternate view. *J. Clim.* **10,** 2351–2357 (1997).
8. Fairbanks, R. G. *et al.* Evaluating climate indices and their geochemical proxies measured in corals. *Coral Reefs* **16,** S93–S100 (1997).
9. Kaplan, A. *et al.* Analyses of global sea surface temperature, 1856–1991. *J. Geophys. Res.* **103,** 18567–18589 (1998).
10. Allan, R., Lindesay, J. & Parker, D. *El Niño Southern Oscillation and Climatic Variability* (CSIRO, Collingwood, 1997).
11. Quinn, W. H., Neal, V. T. & Antuñez de Mayolo, S. E. El Niño occurrences over the past four and a half centuries. *J. Geophys. Res.* **92,** 14449–14461 (1987).
12. Kennedy, J. A. & Brassell, S. C. Molecular records of twentieth-century El Niño events in laminated sediments from the Santa Barbara basin. *Nature* **357,** 62–64 (1992).
13. Dunbar, R. B., Wellington, G. M., Colgan, M. W. & Glynn, P. W. Eastern Pacific sea surface temperature since 1600 AD: The $\delta^{18}O$ record of climate variability in Galapagos corals. *Paleoceanography* **9,** 291–316 (1994).
14. Tudhope, A. W. *et al.* Recent changes in climate in the far western equatorial Pacific and their relationship to the Southern Oscillation: oxygen isotope records from massive corals, Papua New Guinea. *Earth Planet. Sci. Lett.* **136,** 575–590 (1995).
15. Stahle, D. W. *et al.* Experimental dendroclimatic reconstruction of the Southern Oscillation. *Bull. Am. Meteorol. Soc.* **79,** 2137–2152 (1998).
16. Evans, M. N., Fairbanks, R. G. & Rubenstone, J. L. A proxy index of ENSO teleconnections. *Nature* **394,** 732–733 (1998).
17. Cole, J. E., Dunbar, R. B., McClanahan, T. R. & Muthiga, N. Tropical Pacific forcing of decadal variability in the western Indian Ocean over the past two centuries. *Science* **287,** 617–619 (2000).
18. Cole, J. E. & Fairbanks, R. G. The Southern Oscillation recorded in the oxygen isotopes of corals from Tarawa Atoll. *Paleoceanography* **5,** 669–683 (1990).
19. Guilderson, T. P. & Schrag, D. P. Reliability of coral records from the western Pacific warm pool: A comparison using age-optimized records. *Paleoceanography* **4,** 457–464 (1999).
20. Picaut, J., Ioualalen, I., Menkes, C., Delcroix, T. & McPhaden, M. Mechanism of the zonal displacements of the Pacific warm pool: Implications for ENSO. *Science* **274,** 1486–1489 (1996).
21. Trenberth, K. E. & Shea, D. J. On the evolution of the Southern Oscillation. *Mon. Weath. Rev.* **115,** 3078–3096 (1987).
22. Wolter, K. & Timlin, M. S. in *Proc. 17th Climate Diagnostics Workshop* 52–57 (Univ. of Oklahoma, Norman, Oklahoma, 1993).
23. Gagan, M. K., Chivas, A. R. & Isdale, P. J. High-resolution isotopic records from corals using ocean temperature and mass spawning chronometers. *Earth Planet. Sci. Lett.* **121,** 549–558 (1994).
24. Woodruff, S. D., Slutz, R. J., Jenne, R. L. & Steurer, P. M. A comprehensive ocean-atmosphere data set. *Bull. Am. Meteorol. Soc.* **68,** 1239–1250 (1987).
25. Mann, M. E. & Lees, J. Robust estimation of background noise and signal detection in climatic time series. *Clim. Change* **33,** 409–445 (1996).
26. Hughen, K. A., Schrag, D. P. & Jacobsen, S. B. El Niño during the last interglacial period recorded by a fossil coral from Indonesia. *Geophys. Res. Lett.* **36,** 3129–3132 (1999).
27. Mann, M. E., Bradley, R. S. & Hughes, M. K. in *El Niño and the Southern Oscillation: Multiscale Variability and its Impacts on Natural Ecosystems and Society* (ed. Diaz, H. & Markgraf, V.) 321–372 (Cambridge Univ. Press, Cambridge, in the press).
28. Mann, M. E., Bradley, R. S. & Hughes, M. K. Global-scale temperature patterns and climate forcing over the past six centuries. *Nature* **392,** 779–787 (1998).
29. Wellington, G. M., Dunbar, R. B. & Merlen, G. Calibration of stable oxygen isotope signatures in Galápagos corals. *Paleoceanography* **11,** 467–480 (1996).
30. Ropelewski, C. F. & Jones, P. D. An extension of the Tahiti-Darwin Southern Oscillation Index. *Mon. Weath. Rev.* **115,** 2161–2165 (1987).

Acknowledgements

We thank B. Vaughn, T. Kimbell, J. Thurston and the Kiribati Ministry for Natural Resources Development (particularly J. Uan) for logistical assistance. Laboratory analyses were facilitated by C. Evans, J. Kelleher and B. Vaughn. We thank J. White for discussions. Reviews by M. Evans and R. Dunbar greatly improved the manuscript. COADS data are provided by the NOAA-CIRES Climate Diagnostics Centre from their web site at www.cdc.noaa.gov, and with assistance from S. Worley. TAO array data are provided by the TAO Project Office web site at www.pmel.noaa.gov/toga-tao. We thank M. Mann and E. Cook for providing spectral analysis software and advice. This study was supported by the Earth System History Program of the US National Science Foundation and the NOAA Paleoclimatology Program.

Correspondence and requests for materials should be addressed to J.C. (e-mail: jcole@geo.arizona.edu). The bimonthly Maiana $\delta^{18}O$ record is available at http://www.ngdc.noaa. gov/paleo/pubs/urban2000.

Widespread uplift and 'trapdoor' faulting on Galápagos volcanoes observed with radar interferometry

Falk Amelung*†, Sigurjón Jónsson*, Howard Zebker & Paul Segall

Stanford University, Department of Geophysics, Mitchell Building, Stanford, California 94305-2215, USA
**These authors contributed equally to this work.*

Volcanic uplift, caused by the accumulation of magma in subsurface reservoirs, is a common precursor to eruptions[1,2]. But, for some volcanoes, uplift of metres or more has not yet led to an eruption[3]. Here we present displacement maps of volcanoes in the Galápagos Islands, constructed using satellite radar interferometry, that might help explain this dichotomy. We show that all but one of the seven volcanoes on the islands of Isabela and Fernandina deformed during 1992–99. Cerro Azul and Fernandina erupted[4–6] during the observation period and show evidence of inflation, co-eruptive deflation and shallow dyke intrusion. In contrast, the largest volcano, Sierra Negra, has not erupted, yet exhibits spatially and temporally variable deformation, with a maximum uplift of 2.7 m between 1992 and 1999, which can be modelled by a shallow inflating sill. Inflation during 1997–98, however, was accompanied by 'trapdoor' faulting on a steeply dipping fracture system within the caldera. Repeated trapdoor faulting over geological time has formed an arcuate intra-caldera ridge within Sierra Negra and may have acted to relax stresses above the magma chamber, inhibiting summit eruptions. Similar processes may help explain large uplift unaccompanied by eruptive activity at other volcanoes.

A mosaic of two deformation interferograms spanning 1992–7 and 1992–8 shows that all volcanoes on the islands Fernandina and Isabela, except Ecuador, deformed during the observation period (Fig. 1). Ecuador is also the only volcano not to have erupted in historic times (see Table 1). Before these observations there were no instrumental measurements of active deformation in the Galápagos,

† Present address: Hawaii Institute of Geophysics and Planetology, SOEST, University of Hawaii, 2525 Correa Road, Honolulu, Hawaii 96822, USA.

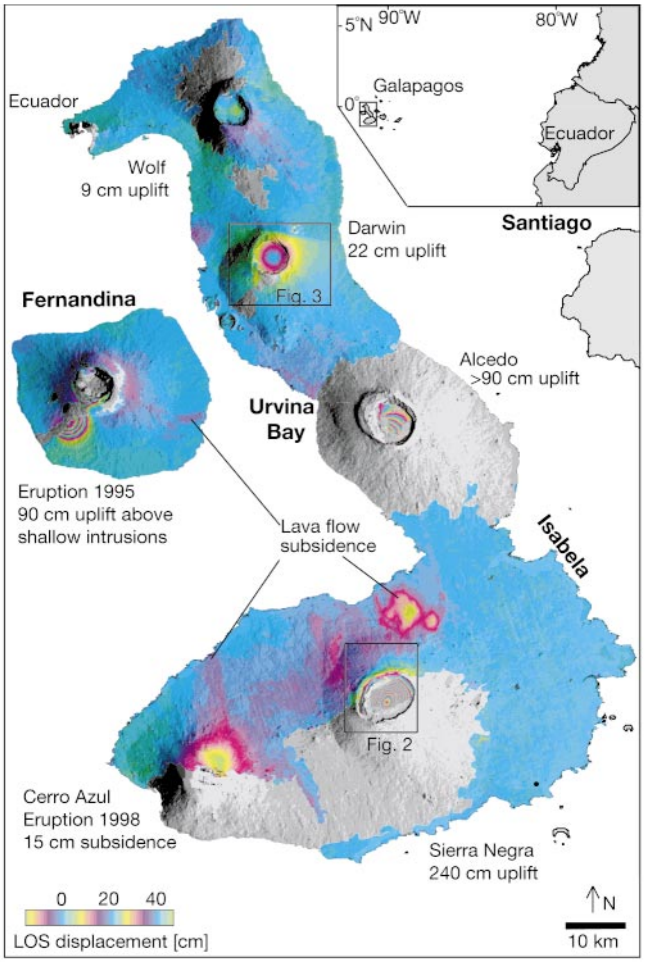

Figure 1 Observed deformation at Isabela and Fernandina (main image), the westernmost islands in the Galápagos archipelago (inset). The map shows line-of sight (LOS) ground displacements towards the European radar satellites ERS-1 and ERS-2, produced from interferograms spanning 5 years from 1992 to 1997 (Ecuador, Wolf, Fernandina) and 6.4 years from 1992 to 1998 (Darwin, Alcedo, Sierra Negra and Cerro Azul; Table 1). The radar echoes are reduced to interferograms by calculating the phase difference between images from two satellite passes[22–24]. The topographic contribution to the observed phase was removed using a digital elevation model[25]. The interferometric phase, which is measured modulo 2π, is unwrapped to[26] produce LOS displacement, and presented here so that each colour-cycle represents 20 cm displacement. The incidence angle of the ERS radars is 23° from vertical. Areas where the interferometric coherence is lost, presumably because of dense vegetation, are shown grey. Also shown is the maximum uplift at each volcano, assuming that displacements are vertical. All the volcanoes actively deformed during the observation period except Ecuador volcano. The 1995 Fernandina eruption occurred on the southwest flank. The 1998 Cerro Azul eruption occurred inside the summit caldera and on the vegetated southeast flank[4].

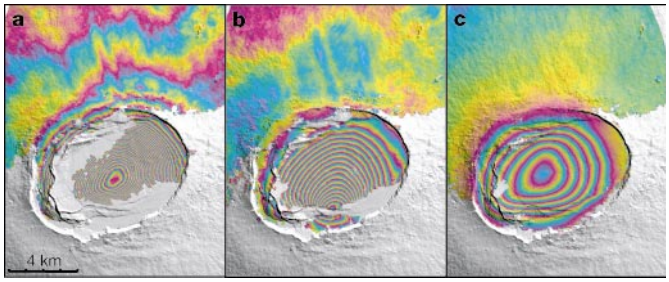

Figure 2 Radar interferograms of Sierra Negra volcano showing uplift during three time periods. **a,** 1992–97 (5.3 years, descending orbit). **b,** 1997–98 (1.1 years, descending orbit). **c,** 1998–99 (0.5 years, ascending orbit). Each colour cycle represents 5 cm LOS displacement. The deformation pattern during the first and third time period is similar, but is markedly different during the intervening period. In **b** the interferometric phase is discontinuous across the pre-existing fault (arcuate ridge) in the southern part of the caldera, the location of the proposed trapdoor faulting.

although 5–7 m of uplift occurred in Urvina Bay in 1954, six months before an eruption of Sierra Negra[7,8]. We derived uplift rates ranging from several millimetres per year at Wolf to 0.9 m per year at Sierra Negra using satellite radar interferometry (InSAR); these rates indicate accumulation of magma in reservoirs beneath the summit calderas of each volcano. Only Cerro Azul and Fernandina erupted during the observation period. At Cerro Azul, pre-eruptive uplift (June 1992 to October 1997), as well as subsidence (October 1997 to November 1998), are associated with the September–October 1998 eruption[4,5]. Fernandina exhibits a semi-circular fringe pattern on its southwest flank (Fig. 1), which has been modelled with a dipping, radial dyke coincident with the 1995 eruption[6]. Uplift of 0.1 m from September 1998 to March 1999 suggests refilling of a shallow magma chamber. Uplift at some volcanoes (for example, Campi Flegrei[9] and Yellowstone[10]) may be related to hydrothermal rather than magmatic processes. Because of the high eruption frequency of the Galápagos volcanoes, and our observations of pre-eruptive uplift and co-eruptive subsidence at Cerro Azul, we suggest that the uplift at the various volcanoes in the Galápagos is due to magma accumulation.

The interferograms also show surprisingly large evidence for subsidence of lava flows on Fernandina, Cerro Azul and Sierra Negra (see Fig. 1). Up to 20 cm of subsidence was observed on the 1979 flows on the north flank of Sierra Negra (between 1992 and 1998), roughly 13–19 years after their emplacement[11]. The subsidence on the north flank of Cerro Azul and on the southeast flank of Fernandina is found on lava flows of unknown age. Potential explanations for the subsidence include thermal contraction, and compaction of the flow, or lava substrate[12–14].

Sierra Negra experienced particularly dramatic and variable ground deformation. We observe a peak radar line-of-sight (LOS) displacement (range decrease) of 2.2 m between 1992 and 1998 (corresponding to 2.4 m of uplift; see Fig. 1) and 0.3 m during the September 1998 to March 1999 period. The corresponding displacement rates vary from 0.32 m yr^{-1} during 1992–97, to 0.90 m yr^{-1} during 1997–98, and 0.65 m yr^{-1} during 1998–99. Figure 2 illustrates that while the spatial pattern of deformation in 1992–97 and 1998–99 was similar, with the maximum uplift near the centre of the caldera, the deformation pattern during the intermediate period (1997–98) was markedly asymmetric with maximum uplift near the south rim of the caldera. Discontinuities in interferometric phase and loss of image coherence coincide with a previously mapped inner caldera fracture system (Fig. 2b). The fracture system, consisting of outward-dipping (60–90°) normal faults, is marked by a 14-km-long curving arcuate ridge, open to the east, which surrounds a tilted and elevated inner caldera floor[11]. We interpret the InSAR data as indicative of faulting along the southern part of the pre-existing fault system during the 1997–98 period. We observed similar fringe discontinuities near intra-caldera faults on Alcedo during 1992–98, but lack of data across the faults and on the volcano's flanks hindered a more detailed analysis.

We inverted the InSAR observations for magma chamber geometry and volume change in an elastic half-space using robust nonlinear optimization methods[15], ignoring second-order effects of elastic and structural heterogeneity, and topography. For Darwin, Wolf and Cerro Azul, point centres of dilation[16] ("Mogi sources") accurately reproduce the near-radial symmetry observed in the fringe pattern (Fig. 3). These models are consistent with magma accumulation in shallow chambers 2–3 km beneath the calderas,

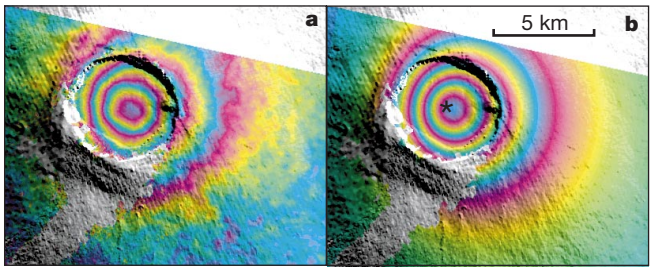

Figure 3 Deformation at Darwin volcano during 1992–98. **a,** Radar interferogram of Darwin volcano showing 0.2 m of LOS displacement (uplift). **b,** Predicted interferogram from the best-fit Mogi model with source location in the centre of the caldera (star) and depth of 3 km. Each colour cycle represents 5 cm LOS displacement. Observations at Wolf and Cerro Azul during 1992–97/98, and at Fernandina during 1998–99 are also well fitted with Mogi models at depths of approximately 2, 5 and 3 km, respectively.

except at Cerro Azul which yields a source depth of about 5 km. Shallow magma accumulation is compatible with inferred depths of fractional crystallization of evolved, well-mixed basalts[17,18]. In contrast with Darwin, Wolf and Cerro Azul, simple point-source models do not accurately describe the data from Sierra Negra or Alcedo. The elliptical deformation pattern and absence of fringes outside the caldera at Sierra Negra require a more realistic magma chamber model than a Mogi source (Fig. 4a and b).

The radar data alone cannot uniquely resolve the shape of what are undoubtedly complex magma chambers, but we can fit the data with geologically plausible sources of deformation. The Sierra Negra data from the first and third time periods (Fig. 2a and c) can be fitted with a sill whose opening varies spatially. We first assume a horizontal sill with uniform opening and solve for the length, width, depth and opening. We retain the optimal depth of 1.9 km, enlarge the surface area, and solve for the spatial distribution of opening. We find a distribution of opening that fits the radar data in a least-squares sense, is reasonably smooth, and constrains the opening to be non-negative[19]. We found openings of up to 0.5 m between September 1998 and March 1999 (Fig. 4c and d). The magma body itself may be much thicker as the data are only sensitive to the change in thickness. This model is geologically reasonable and provides a much better fit to the observations than the point-source model (Fig. 4).

The 1997–98 observations at Sierra Negra (Fig. 2b) require a combination of two processes: uplift due to the expanding magma body and faulting along the inner caldera fracture system. We model the data with uniform sill opening and allow slip on a 75° dipping normal fault coincident with the mapped fracture system[11] (Fig. 5). We found fault slip of up to 1.2 m; the estimated seismic moment would correspond to an earthquake of magnitude 5.7 (ref. 20),

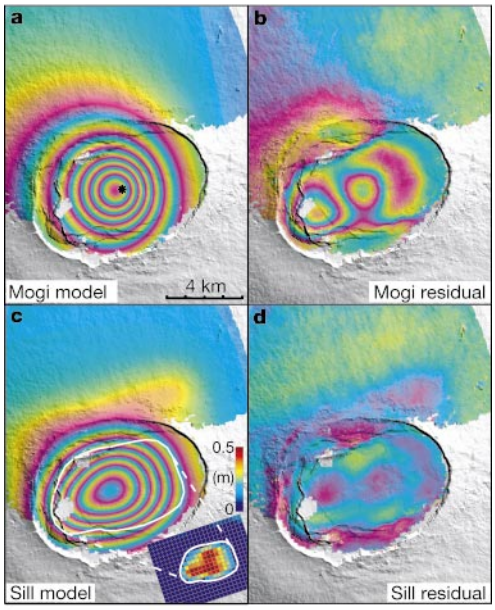

Figure 4 Two models for the Sierra Negra deformation during 1998–99. See data in Fig. 2c. **a,** Best-fit Mogi model. **b,** The residual, the difference between the data and the Mogi model prediction; large residual indicates a poor fit. **c,** Model of a horizontal sill at 1.9 km depth with variable openings of up to 0.5 m (shown in the lower right corner). **d,** The corresponding residual between the data and the sill model. The deformation on Sierra Negra from 1992–97 (Fig. 2a) is likewise better described by a sill than by a point-source model.

assuming a shear modulus of 30 GPa. The largest reported earthquake in the Sierra Negra area during this time interval was a M_w = 5.0 event on 11 January 1998 (see data from the National Earthquake Information Center (NEIC) at http://wwwneic.cr.usgs.gov/). Unless the shear modulus of the near surface rocks is an order of magnitude less than assumed, this earthquake accounts for only 8% of the estimated moment release, suggesting that the slip was predominantly aseismic. Fault slip allowed the crust above the magma body to hinge upward like a trapdoor, with the sill opening occurring north of the normal fault system.

Uplift before 1997–98 caused extension of the caldera floor, eventually leading to trapdoor faulting sometime in 1997–98. The stress perturbations caused by magma chamber pressurization were thus sufficient to initiate slip on the fault, although conditions for a dyke to propagate to the surface were not achieved. Slip on the arcuate fault system apparently relaxed shear stresses along the fault because slip was not observed between 1998 and 1999, although uplift continued. Cumulative vertical offsets along the arcuate fault structure observed in the topography range from 10 m in the area of

Table 1 Maximum line-of-sight displacements at various volcanoes

Volcano	Last eruption	Track 140 6/15/92–10/16/97 5.3 years $\mathbf{B}_\perp$ = 453 m	Track 140 10/16/97–11/5/98 1.1 years $\mathbf{B}_\perp$ = 367 m	Track 140 6/15/92–11/5/98 6.4 years† $\mathbf{B}_\perp$ = 85 m	Track 412 9/12/92–9/30/97 5 years* $\mathbf{B}_\perp$ = 279 m	Track 61 9/26/98–3/20/99 0.5 years $\mathbf{B}_\perp$ = 5 m
Ecuador	Not known[21]	–	–	–	0	–
Wolf	1982[8]	–	–	–	0.08 m	–
Femandina	1995[6]	–	–	–	0.85 m†	0.08 m
Darwin	1812[8]	0.17 m	<0.05 m	0.20 m	0.14 m	<0.03 m
Alcedo	~1946–1960[7]	>0.80 m	<0.05 m	>0.85 m	–	<0.03 m
Sierra Negra	1979[11]	1.59 m	0.90 m	2.20 m	–	0.30 m
Cerro Azul	1998[5]	0.13 m	–0.26 m†	–0.14 m*	–	<0.03 m

Data was observed in five different interferograms derived from nine available radar scenes acquired in 1992 and in 1997–99. $\mathbf{B}_\perp$ is the perpendicular component of the spatial separation between two satellite passes. Images from track 140 and 412 are acquired from descending satellite orbits and the images from track 61 from ascending orbits.
* In Fig. 1.
† Eruption occurred during this time period.

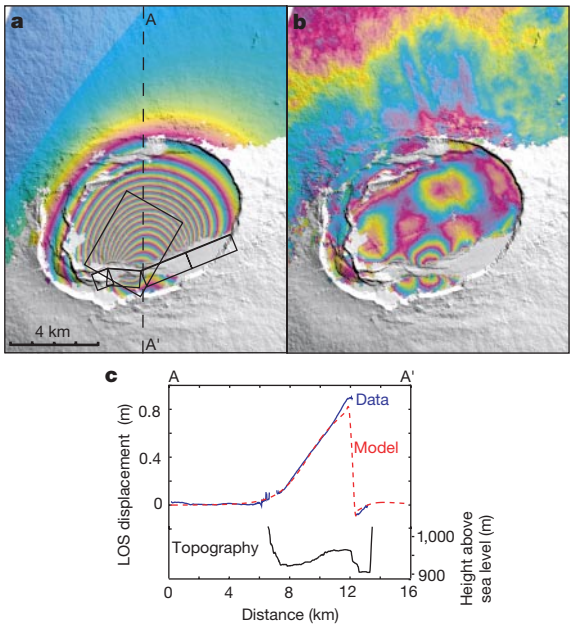

Figure 5 Model for the observed deformation on Sierra Negra during 1997–98. See Fig. 2b. **a,** The model has uniform opening of a horizontal sill (large rectangle) and slip on the normal faults that bound the elevated inner caldera floor. The four smaller rectangles show the surface projection of normal fault patches used in the modelling; a thick line marks the upper edge. The depth of the sill is not well constrained in this case; estimates range between 2.3 and 2.9 km. The difference between this and the depth obtained when trapdoor faulting was not present (2.2 km in 1992–97 and 1.9 km in 1998–99) is unlikely to be significant owing to imperfect resolution and model approximations. **b,** Residual between the data and the model prediction. Localized fringes near the fault are due to the simplified representation of the fault as four rectangular dislocation segments. **c,** Comparison between the data and the model showing the LOS displacement along the profile A–A′ as well as the intra-caldera surface topography. The observed displacement follows the topography indicating repeated slip events.

maximum uplift in 1997–98 to over 100 m in the western caldera. In places the ridge actually extends above the caldera rim, indicating that trapdoor faulting has occurred numerous times since the caldera floor was resurfaced. The last four eruptions (and perhaps more) were not intra-caldera eruptions but occurred in the area north of the caldera. Our observations suggest that repeated slip on intra-caldera (or caldera bounding) faults may allow uplift without accumulating sufficient stress to permit vertical dyke propagation. Similar processes may explain large uplifts without eruptions at other rapidly deforming volcanoes[3]. □

Received 3 March; accepted 24 August 2000.

1. Dvorak, J. J. & Dzurisin, D. Volcano geodesy: the search for magma reservoirs and the formation of eruptive vents. *Rev. Geophys.* **35,** 343–384 (1997).
2. Lipman, P. W., Moore, J. G. & Swanson, D. A. Bulging of the north flank before the May 18 eruption–geodetic data. *USGS Prof. Pap.* **1250,** 143–155 (1981).
3. Newhall, C. G. & Dzurisin, D. Historical unrest at large calderas of the world. *USGS Bull.* **1855,** 509–520 (1988).
4. Naumann, T. & Geist, D. Physical volcanology and structural development of Cerro Azul Volcano, Isabela Island, Galápagos: Implication for the development of Galápagos-type shield volcanoes. *Bull. Volcanol.* **61,** 497–514 (2000).
5. Mouginis-Mark, P. J., Snell, H. & Ellisor, R. GOES satellite observations of the 1998 eruption of Volcan Cerro Azul, Galápagos Islands. *Bull. Volcanol.* **62,** 188–198 (2000).
6. Jónsson, S. *et al.* A shallow-dipping dike fed the 1995 flank eruption at Fernandina volcano, Galápagos, observed by satellite radar interferometry. *Geophys. Res. Lett.* **26,** 1077–1080 (1999).
7. Geist, D., Howard, K. A., Jellinek, A. M. & Rayder, S. The volcanic history of Volcán Alcedo, Galápagos Archipelago: A case study of rhyolitic oceanic volcanism. *Bull. Volcanol.* **56,** 243–260 (1994).
8. Simkin, T. & Siebert, L. *Volcanoes of the World* 2nd edn (Geoscience, Tucson, 1994).
9. Bonafede, M. & Mazzanti, M. Modelling gravity variations consistent with ground deformation in the Campi Flegrei caldera (Italy). *J. Volcanol. Geotherm. Res.* **81,** 137–157 (1998).
10. Wicks, C. Jr, Thatcher, W. & Dzurisin, D. Migration of fluids beneath Yellowstone caldera inferred from satellite radar interferometry. *Science* **282,** 458–462 (1998).
11. Reynolds, R. W., Geist, D. & Kurz, M. D. Physical volcanology and structural development of Sierra Negra volcano, Isabela island, Galápagos archipelago. *Geol. Soc. Am. Bull.* **107,** 1398–1410 (1995).
12. Murray, J. B. The influence of loading by lavas on the siting of volcanic eruption vents on Mt Etna. *J. Volcanol. Geotherm. Res.* **35,** 121–139 (1988).
13. Briole, P., Massonnet, D. & Delacourt, C. Post-eruptive deformation associated with the 1986–87 and 1989 lava flows on Etna detected by radar interferometry. *Geophys. Res. Lett.* **24,** 37–40 (1997).
14. Stevens, N. F. Surface movements of emplaced lava flows measured by SAR interferometry. *J. Geophys. Res.* (in the press).
15. Cervelli, P., Murray, M. H., Segall, P., Aoki, Y. & Kato, T. Estimating source parameters from deformation data, with an application to the March 1997 earthquake swarm off the Izu Peninsula, Japan. *J. Geophys. Res.* (in the press).
16. Mogi, K. Relations between the eruptions of various volcanoes and the deformation of the ground surface around them. *Bull. Earth. Res. Inst. Univ. Tokyo* **36,** 99–134 (1958).
17. Geist, D., Naumann, T. & Larson, P. Evolution of Galápagos magmas: Mantle and crustal level fractionation without assimilation. *J. Petrol.* **39,** 953–971 (1998).
18. Allen, J. F. & Simkin, T. Fernandina Volcano's evolved, well-mixed basalts: Mineralogical and petrological constraints on the nature of the Galápagos plume. *J. Geophys. Res.* **105,** 6017–6041 (2000).
19. Lawson, C. L. & Hanson, R. J. *Solving Least Squares Problems* (Prentice-Hall, Englewood Cliffs, New Jersey, 1974).
20. Kanamori, H. & Anderson, D. L. Theoretical basis of some empirical relations in seismology. *Bull. Seismol. Soc. Am.* **65,** 1073–1095 (1975).
21. Rowland, S., Munro, D. C. & Perez-Oviedo, V. Volcán Ecuador, Galápagos islands: erosion as a possible mechanism for the generation of steep-sided basaltic volcanoes. *Bull. Volcanol.* **56,** 271–283 (1994).
22. Massonnet, D. *et al.* The displacement field of the Landers earthquake mapped by radar interferometry. *Nature* **364,** 138–142 (1993).
23. Zebker, H., Rosen, P., Goldstein, R., Gabriel, A. & Werner, C. On the derivation of coseismic displacement fields using differential radar interferometry: The Landers earthquake. *J. Geophys. Res.* **99,** 19617–19643 (1994).
24. Massonnet, D. & Feigl, K. Radar interferometry and its application to changes in the Earth's surface. *Rev. Geophys.* **36,** 441–500 (1998).
25. Mouginis-Mark, P. J., Rowland, S. K. & Garbeil, H. Slopes of western Galápagos volcanoes from airborne interferometric radar. *Geophys. Res. Lett.* **23,** 3767–3770 (1996).
26. Goldstein, R. M., Zebker, H. A. & Werner, C. L. Satellite radar interferometry: Two-dimensional unwrapping. *Radio Sci.* **23,** 713–720 (1988).

Acknowledgements

We thank the European Space Agency for providing the SAR data and for supporting F.A. with a post-doctoral fellowship. This study was also supported by NASA. We thank D. Geist and P. Lundgren for comments.

Correspondence and requests for materials should be addressed to S.J. (e-mail: jonsson@pangea. stanford. edu) or F.A. (e-mail: amelung@pgd. hawaii. edu).

Unicellular C_4 photosynthesis in a marine diatom

John R. Reinfelder*, Anne M. L. Kraepiel† & François M. M. Morel‡

* *Department of Environmental Sciences, Rutgers University, 14 College Farm Road, New Brunswick, New Jersey 08901, USA*
† *Centre de Geochimie de la Surface, Université de Strasbourg, 1 rue Blessig, 67084 Strasbourg, France*
‡ *Department of Geosciences, Princeton University, Princeton, New Jersey 08544, USA*

Nearly 50 years ago, inorganic carbon was shown to be fixed in microalgae as the C_3 compound phosphoglyceric acid[1]. The enzyme responsible for C_3 carbon fixation, ribulose-1,5-bisphosphate carboxylase (Rubisco), however, requires inorganic carbon in the form of CO_2 (ref. 2), and Rubisco enzymes from diatoms have half-saturation constants for CO_2 of 30–60 μM (ref. 3). As a result, diatoms growing in seawater that contains about 10 μM CO_2 may be CO_2 limited[4]. Kinetic and growth studies have shown that diatoms can avoid CO_2 limitation[5–7], but the biochemistry of the underlying mechanisms remains unknown. Here we present evidence that C_4 photosynthesis supports carbon assimilation in